Live-cell fluorescence correlation spectroscopy dissects the role of coregulator exchange and chromatin binding in retinoic acid receptor mobility

Peter Brazda[1], Tibor Szekeres[2], Balázs Bravics[2], Katalin Tóth[3], György Vámosi[2,*,‡] and Laszlo Nagy[1,4,*,‡]

[1]Department of Biochemistry and Molecular Biology, University of Debrecen, Medical and Health Science Centre, Research Centre for Molecular Medicine, Egyetem ter 1. Debrecen, H-4010, Hungary
[2]Cell Biology and Signaling Research Group of the Hungarian Academy of Sciences, Department of Biophysics and Cell Biology, University of Debrecen, Medical and Health Science Centre, Research Centre for Molecular Medicine, Nagyerdei krt. 98. Debrecen, H-4012, Hungary
[3]German Cancer Research Center, Division Biophysics of Macromolecules, Im Neuenheimer Feld 580, D-69120 Heidelberg, Germany
[4]Apoptosis and Genomics Research Group of the Hungarian Academy of Sciences, University of Debrecen, Medical and Health Science Centre, Research Centre for Molecular Medicine, Egyetem tér 1. Debrecen, H-4010, Hungary

*Authors for correspondence (nagyl@med.unideb.hu; vamosig@dote.hu)
‡These authors contributed equally to this work

Accepted 13 June 2011
Journal of Cell Science 124, 3631–3642

doi: 10.1242/jcs.086082

Summary

The retinoic acid receptor (RAR) is a member of the nuclear receptor superfamily. This ligand-inducible transcription factor binds to DNA as a heterodimer with the retinoid X receptor (RXR) in the nucleus. The nucleus is a dynamic compartment and live-cell imaging techniques make it possible to investigate transcription factor action in real-time. We studied the diffusion of EGFP–RAR by fluorescence correlation spectroscopy (FCS) to uncover the molecular interactions determining receptor mobility. In the absence of ligand, we identified two distinct species with different mobilities. The fast component has a diffusion coefficient of $D_1=1.8-6.0$ μm^2/second corresponding to small oligomeric forms, whereas the slow component with $D_2=0.05-0.10$ μm^2/second corresponds to interactions of RAR with the chromatin or other large structures. The RAR ligand-binding-domain fragment also has a slow component, probably as a result of indirect DNA-binding through RXR, with lower affinity than the intact RAR–RXR complex. Importantly, RAR-agonist treatment shifts the equilibrium towards the slow population of the wild-type receptor, but without significantly changing the mobility of either the fast or the slow population. By using a series of mutant forms of the receptor with altered DNA- or coregulator-binding capacity we found that the slow component is probably related to chromatin binding, and that coregulator exchange, specifically the binding of the coactivator complex, is the main determinant contributing to the redistribution of RAR during ligand activation.

Key words: FCS, RAR, Diffusion, Nuclear receptor

Introduction

Nuclear receptors are transcription factors that are able to regulate the expression of their target genes by direct DNA-binding in a ligand-dependent manner. An important subgroup of this protein superfamily is that of retinoid receptors including retinoic acid (RARα, RARβ and RARγ) and retinoid x receptors (RXRα, RXRβ and RXRγ), which play a central role in endocrine signaling, regulation of embryonic and adult development, and myeloid cell differentiation (Mangelsdorf et al., 1995). RXR acts as a heterodimerization partner for several types of nuclear receptors. Retinoid receptors possess two well-conserved domains present in all nuclear receptors: the DNA-binding domain (DBD) and the ligand-binding domain (LBD) at the C-terminus of the protein. The DBD contains two zinc-finger motifs and is linked to the LBD by a highly flexible hinge region. The LBD shows a greater diversity among nuclear receptors because it is a site for receptor-specific ligand binding. It possesses transactivation activity through the activation function 2 (AF-2) domain and contains a ligand-binding pocket as well as the main interaction surfaces for dimerization and coregulator binding. The C-terminal helix (H12) of the LBD was found to be essential for coregulator exchange (Love et al., 2002).

Our current view of nuclear receptor action is largely defined by the rather rigid molecular switch model, which describes the course of events taking place during activation of receptors (Nagy et al., 1999). According to this model, retinoid receptors are bound to both DNA and corepressors in the unliganded (repressed) state. SMRT (silencing mediator of retinoic acid and thyroid hormone receptor) and N-COR (nuclear receptor corepressor) are key corepressors in this system and they harbor two interaction domains (IDs) that make direct interaction with nuclear receptors possible. At the same time, these corepressors can also serve as docking sites for additional components of a corepressor complex such as histone deacetylases, allowing the formation of large protein complexes (Chen and Evans, 1995). Based on structural studies, the model proposes that ligand binding induces a more tightly packed conformation of the receptor with the H12 bound to the receptor's surface. In this new conformation, the receptor has a decreased affinity towards corepressors and acquires a binding surface for coactivators such as ACTR (activator for thyroid

hormone and retinoid receptors) or DRIP/TRAP (Onate et al., 1995; Heery et al., 1997; Darimont et al., 1998; Rachez et al., 1998). The coactivator serves as a docking surface for additional components of the activator complex, histone acetyltransferases, chromatin remodeling factors and the basic transcriptional machinery (Gottlicher et al., 1998; Hermanson et al., 2002). This model suggests a rather rigidly predetermined sequence of events taking place on the receptor, which is sitting statically on its response element.

As a result of the ever increasing number of identified coregulators, and the numerous complexes with which they can associate, it has become evident that there must be some functional redundancy and a greater flexibility in coregulator–receptor interactions. The potential of combinatorial regulation, the high 3D flexibility of receptors and the determining role of local nuclear architecture all point towards the formulation of a more flexible and dynamic model. Most importantly, the contribution of diffusion and mobility in the nucleus has not been accounted for in most of the models proposed, which have been largely based on transfection and biochemical analyses, as well as protein structures (Sprague et al., 2004).

However, biophysical methods such as fluorescence recovery after photobleaching (FRAP) studies opened up the sub-second range of events by reporting that glucocorticoid receptors (GRs) show characteristic residence times of seconds on response element arrays. This challenge of the rigid model of stably formed complexes bound to DNA led to the proposal of the hit-and-run model, suggesting the existence of a highly dynamic system (McNally et al., 2000). The immobile fraction and half-recovery time of labeled molecules give a hint about their dynamics. By developing more elaborate diffusion models for FRAP, it is now becoming possible to distinguish several diffusion components (Axelrod et al., 1976; Lippincott-Schwartz et al., 2003). However if a mixture of distinct populations were analyzed as a single species, the calculated average diffusion time would not represent a biologically meaningful parameter, or would at least obscure the real molecular behavior of the system.

Somewhat contrary to these results, which suggest rapid exchange of transcription factors on the promoter, systematic chromatin immunoprecipitation (ChIP) experiments were able to show the cyclic features of the mobility of chromatin remodeling proteins and transcription factors on the time scale of tens of minutes (Hinojos et al., 2005; Metivier et al., 2006). As it was pointed out, the latter findings might reflect different equilibrium states and their changes, but not the dynamic behavior of these proteins (Gelman et al., 2006). These studies clearly suggest that further biophysical analysis of the diffusion of these molecules is necessary.

To study and measure multicomponent diffusion, we applied fluorescence correlation spectroscopy (FCS), which is a fluorescence microscopy technique having single-molecule sensitivity. It uses the fluctuation of fluorescence intensity resulting from the diffusion of fluorescently labeled molecules in and out of a confocal (subfemtoliter-sized) volume (Brock et al., 1999; Vamosi et al., 2009). The recorded fluorescence signal is used to extract an autocorrelation function (ACF), which reflects the photophysical and diffusion properties of the molecules. By fitting the autocorrelation curves to various diffusion models, it is possible to determine diffusion times, calculate diffusion coefficients and the fractions of molecules in each subpopulation characterized by distinct diffusion parameters (Lippincott-Schwartz et al., 2001; Hess and Webb, 2002; Bacia and Schwille, 2003; Berland, 2004). To monitor the dynamic features of human RARα (referred to as RAR here), expression vectors coding for the fusion proteins of fluorophores (EGFP, mCherry) and the receptor (human RARα) or coregulator (ACTR, SMRT) interaction domains were constructed. We found a fast population corresponding to smaller complexes or dimers, and a slow population, which probably reflects chromatin binding. By mapping the diffusion behavior of various functional mutants of the receptor with altered DNA- or coregulator-binding capacities, we have defined the factors determining receptor mobility. Ligand-induced transition to the slow population depends on the co-activator binding capacity of the receptor.

Results

Two distinct populations of EGFP–RAR with different mobility are indicated by fits of FCS autocorrelation curves

Our first aim was to determine the main characteristics of RAR mobility in single cells using FCS. For these studies, we used HeLa cells stably expressing EGFP–RAR. Confocal microscopic images of EGFP–RAR showed clear nuclear localization and a homogenous distribution within the nucleus (Fig. 1A). By contrast, the truncated form, comprising the LBD only, was also present in the cytoplasm (Fig. 1B). Each form was excluded from the nucleoli. The averaged autocorrelation curves were fitted to different types of diffusion models: one-component free diffusion, one-component anomalous diffusion and two-component free diffusion. The residuals show systematic deviations for the one-component fits (Fig. 2A,B). In addition, they also have larger chi-square values than the two-component fit. Chi-square values were the lowest for the two-component model for the different mutant forms of the receptor as well (supplementary material Table S1). Comparison of the one-component free diffusion, two-component free diffusion and one-component anomalous diffusion models with F-test or corrected Aikaike's Information Criteria also supported the two-component model. Nuclear receptors participate in various complexes during their function; thus a multicomponent model is plausible. We also tested a two-component anomalous diffusion model. The anomaly parameters showed large standard deviation (data not shown), including values $\alpha>1$ for the fast component, hinting at directed motion, which we cannot interpret in our model system.

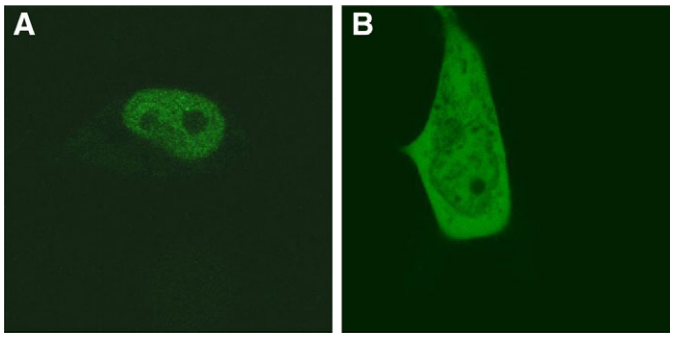

Fig. 1. Localization of EGFP–RAR. Confocal images of HeLa cells expressing (**A**) EGFP–RAR or (**B**) EGFP–RAR-LBD taken with an Olympus FV 1000 microscope (EGFP fluorescence, Ex. 488 nm, Em. 500–530 nm).

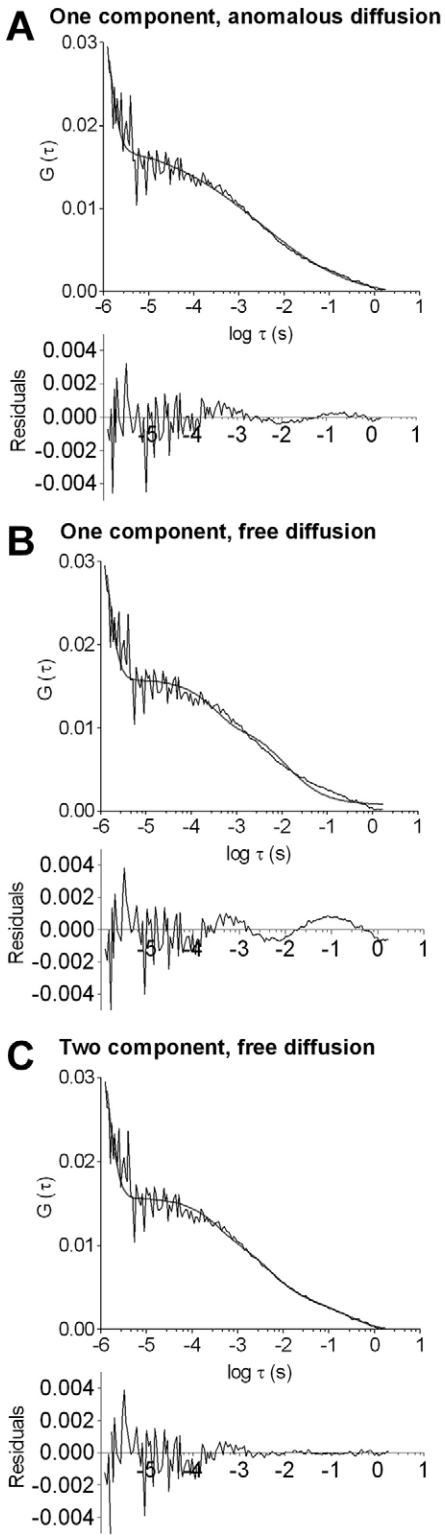

Fig. 2. Nonlinear fitting of EGFP–RAR autocorrelation curves to diffusion models. (**A**) Fit of EGFP–RAR FCS autocorrelation curve with the one-component, anomalous-diffusion model. Below the residuals are shown (χ^2=33). (**B**) Fit with the one-component, free-diffusion model (χ^2=103). (**C**) Fit with the two-component, free-diffusion model (χ^2=26).

Thus, autocorrelation curves of EGFP–RAR were accounted for by a two-component free diffusion model, which gave a tight fit throughout the curve (Fig. 2C). Including a third diffusion component did not improve the fit, or had such a low amplitude that no reliable diffusion time could be determined. Mobility parameters for the wild-type and mutant receptors derived from the two-component free diffusion model are shown in Table 1. (For a comparison of mobility parameters determined by the two-component free diffusion and one-component anomalous models, see supplementary material Table S2.)

Diffusion times were in the range of τ_1=1.5–5 mseconds and τ_2=75–150 mseconds for the faster and the slower population corresponding to diffusion coefficients of D_1=1.8–6 μm^2/second and D_2=0.06–0.12 μm^2/second, respectively. We also determined the diffusion time and diffusion coefficient of EGFP alone (D=13 μm^2/second), according to the one-component free diffusion model. (The fits of a representative EGFP autocorrelation curve and the residuals of the fits are shown in supplementary material Fig. S1.) From the diffusion times we assessed the masses of the diffusing complexes (see Eqn 5 in the Materials and Methods). These calculations were based on assuming a spherical shape for the complex, which may not hold exactly true, but allows an estimation of the order of magnitude of the mass.

The apparent molecular masses of diffusing EGFP–RAR complexes were calculated by comparing their diffusion times with that of EGFP. The apparent masses for both populations turned out to be larger than that of a monomeric EGFP–RAR, 51 kDa. The ratio of this apparent molecular mass and the real molecular mass gives us the number of receptors (or molecules in the complex having an equivalent mass) that are expected to have the measured diffusion time. This ratio is 5–10 in the fast population, which might represent receptor oligomers or receptors bound to smaller complexes. In the case of the slower population, this ratio is as high as 10^6 (Fig. 3A). The existence of such a large diffusing complex is unlikely, suggesting that transient or stable interactions with the chromatin or other practically immobile structures take place.

Considering a two-component model, another important aspect is the distribution of receptors among the fast and slow populations. r_1 describes the fraction of molecules with the shorter diffusion times (‘fast population’) and r_2 represents the fraction with the larger diffusion times (‘slow population’), summing up to 100%. For a complete overview of the distributions of the diffusion times we plotted their relative frequency histograms (Fig. 3B). As shown, ~30% of EGFP–RAR belongs to the slow population in absence of ligand (Fig. 3C). Neither the diffusion times, τ_1 and τ_2, nor their population ratios, r_1 and r_2, showed any correlation with the average number of molecules (N) in the detection volume characterizing the concentration (supplementary material Fig. S2A–C). This proves that the detected diffusion times and the fractions of slow and fast species are not due to artifacts such as large aggregates that could occur as a result of overexpression. In our analysis we included only measurements where the value of N was in the range of 20–50. EGFP–RAR-expressing cells showed a threefold increase in RAR mRNA level compared with levels in the nontransfected cells, as determined by quantitative RT-PCR (supplementary material Fig. S3). RAR protein expression increased twofold in cells stably transfected with GFP–RAR, as shown by immunofluorescence imaging (supplementary material Fig. S4, Table S3).

Table 1. Mobility parameters of wild type and mutant EGFP–RAR

	100 nM AM580	τ_1 (mseconds)	r_2	τ_2 (mseconds)	n
EGFP–RAR	–	2.64±0.65	29±7%	97±57	420
EGFP–RAR	+	2.87±0.99	43±9%	89±45	340
EGFP–RAR-A392R	–	2.69±0.73	27±8%	108±81	117
EGFP–RAR-A392R	+	2.83±0.92	39±11%	92±56	80
EGFP–RAR-W225A	–	2.64±1.07	22±8%	119±81	90
EGFP–RAR-W225A	+	2.54±0.5	26±7%	127±80	87
EGFP–RAR-V395A	–	2.66±1.29	20±8%	120±112	130
EGFP–RAR-V395A	+	2.65±0.84	19±9%	116±121	140
EGFP–RAR-dH12	–	2.83±0.81	26±7%	120±62	130
EGFP–RAR-dH12	+	3.17±0.84	27±7%	124±58	130
EGFP–RAR-mZn	–	2.89±0.7	29±6%	105±61	130
EGFP–RAR-mZn	+	3.40±0.99	35±9%	111±61	110
EGFP–RAR-LBD	–	1.62±0.62	17±11%	99±101	150
EGFP–RAR-LBD	+	2.05±1.20	27±15%	114±138	150

Data represent the parameters of EGFP–RAR before (−) and 10 minutes after (+) the addition of 100 nM AM580 derived from fitting all the measurements done to the two-component free diffusion model. Data are mean ± s.d. In each cell, two to three points were selected for FCS measurements. Thus n values represent ~2–3× the number of measured cells.

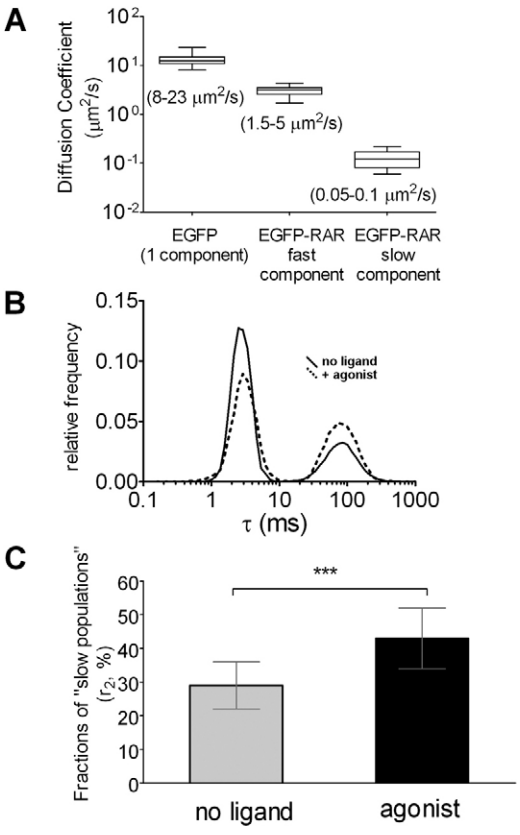

Fig. 3. Mobility parameters of EGFP–RAR. (**A**) Diffusion coefficients of the EGFP molecule determined by the one-component free-diffusion model, compared with the fast and slow component of EGFP–RAR molecule, determined by the two-component free-diffusion model. Fast population: τ_1=1.5–5 mseconds, D_1=1.8–6 μm²/second. Slow population: τ_2=75–150 mseconds, D_2=0.05–0.1 μm²/second. (**B**) Distribution of diffusion times of EGFP–RAR before (solid line) and 10 minutes after (dotted line) the addition of 100 nM AM580. (**C**) Fraction of the slow population before (gray) and 10 minutes after (black) addition of 100 nM AM580 (data are means ± s.d.; ***P<0.001).

Activation of RAR changes population ratios but not diffusion times

A central concept of nuclear receptor action is the molecular switch model describing ligand-dependent coregulator exchange as the main event that makes activation possible. Next, we investigated how this event is reflected by the mobility of RAR. Treatment with a saturating concentration of a selective RAR agonist (100 nM AM580) caused only a slight change in diffusion times. As the diffusion time distribution histogram shows, it is the transition from the fast to the slow population rather than the change of the diffusion times that principally hallmarks receptor activation. As a result of agonist treatment, a significant, ~10% increase was detected in the ratio of the slow population (Fig. 3B,C). The increase of r_2 was found to be specific for the RAR-agonist. No change of r_2 was detected after RAR antagonist (AGN109) treatment, indicating that enhanced co-repressor binding is not influencing the mobility and distribution of the receptors and also confirms the absence of endogenously produced agonist ligands. In addition, treatment with RXRα agonist (LG268) or PPARγ agonist (Rosiglitazone) also induced no change, showing the specificity of RAR-selective ligand treatment (Fig. 4A). The RAR-agonist-induced increase of r_2 was detectable as early as 10 minutes after treatment, and was still present 120 minutes later. This effect was detectable for AM580 concentrations >1 nM, and was saturated around 10–100 nM (Fig. 4B). The increase of r_2 persisted even after washing out the ligand with ligand-free medium (Fig. 4C). Based on these results 100 nM ligand concentration was used for receptor activation in subsequent FCS experiments.

Changing coregulator-binding capacity alters the equilibrium between the fast and slow components

The characteristic change correlated with ligand-dependent RAR activation is the increase of the slow population r_2; thus our aim was to find the key factors that determine this phenomenon. According to the molecular switch model of nuclear receptors, the main feature of the mechanism is coregulator exchange, which could also affect receptor dynamics. The process of receptor activation consists of corepressor release and subsequent coactivator binding, accompanied by a conformational change of the receptor. Previously, we reported that mutations of RAR

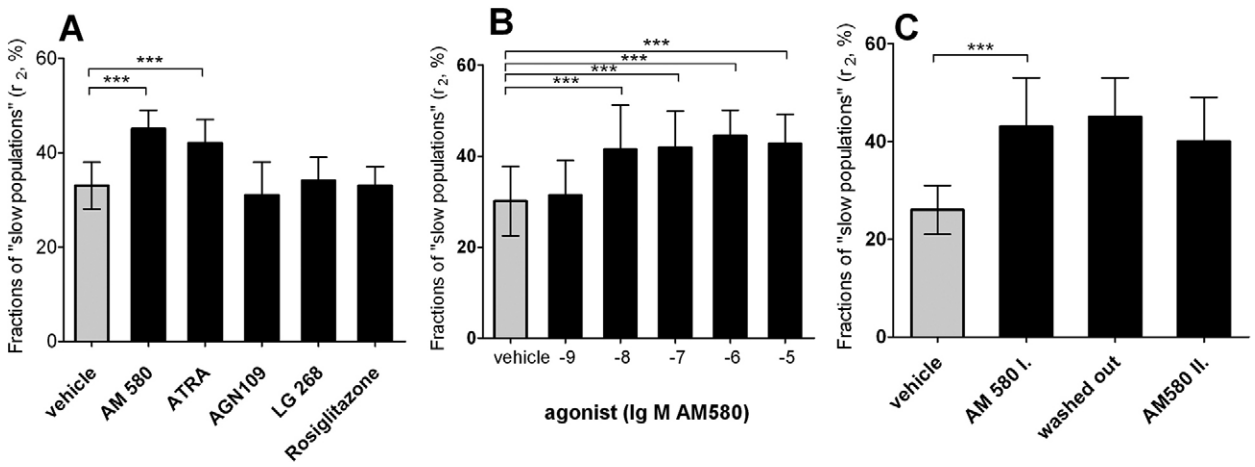

Fig. 4. Dependence of population ratios of EGFP–RAR on type and dose of ligand, and mode of activation. (**A**) Fraction of the slow population (r_2) before (gray, vehicle) and after addition of 100 nM of the indicated ligands: synthetic (AM580) and natural (ATRA, all-trans retinoic acid) RARα-agonists, RARα-antagonist (AGN109), synthetic RXRα-agonist (LG268) and PPARγ-agonist (Rosiglitazone). (**B**) Dose dependence of the rearrangement of EGFP–RAR population ratios 10 minutes after addition of (10^{-9} to 10^{-5} M) AM580. (**C**) Fraction of the slow population following pulsed ligand treatment. No ligand, before ligand treatment; AM580 I, 10 minutes after the addition of 100 nM AM580 for the first time; washed out, 20 minutes after the medium was replaced with ligand-free medium; AM580 II, 10 minutes after the second AM580 treatment (data are means ± s.d.; ***P<0.001).

affect co-factor binding in specific ways (Benko et al., 2003). Based on this knowledge, we created a series of (EGFP-fused) point mutants modified at the surface residues of the fourth and eleventh helix of the RAR ligand-binding domain (Fig. 5). RAR-A392R is reported to be a mutant with an affinity for coactivators higher than that of the wild type. Its 'apo' (unliganded) form is unable to bind corepressor, but shows an increased affinity for coactivators. The latter interaction gets even more robust when agonist is present. This mutant had an increased transactivating ability compared with that of the wild type (supplementary material Fig. S5). RAR-W225A shows an increased affinity for the SMRT corepressor, thus being unable to release it upon ligand treatment. Therefore, agonist-dependent coregulator exchange cannot take place, rendering this mutant to lose its activity (supplementary material Fig. S5). RAR-V395A shows a greatly reduced affinity for corepressors as well as coactivators and is called a no-coregulator-binding mutant. All the point mutants showed nuclear localization and a distribution that was

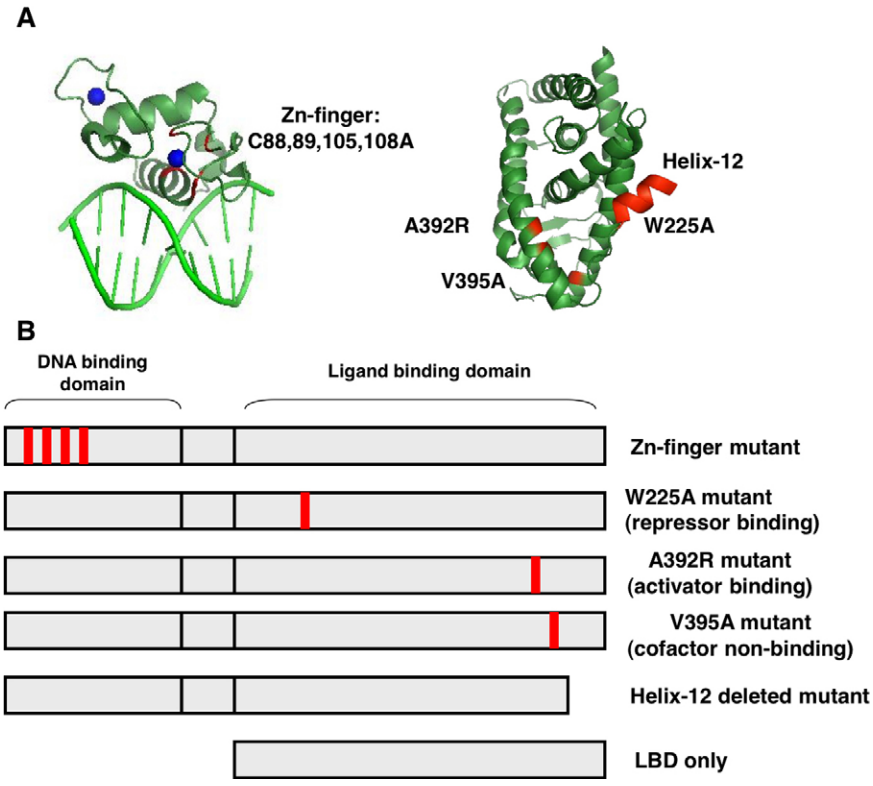

Fig. 5. Representation of mutant forms of RAR. (**A**) Ribbon representation of RAR ligand binding domain (PDB number, 3KMZ), showing the positions of W225A, V240A and A392R mutations and RAR DNA binding domain with its response element (PDB number, 1YNW), showing the positions of the four cysteines (red) within the first zinc-finger that were substituted with alanines. (**B**) Schematic representation of the RAR molecules used in this study (the EGFP moiety is not shown).

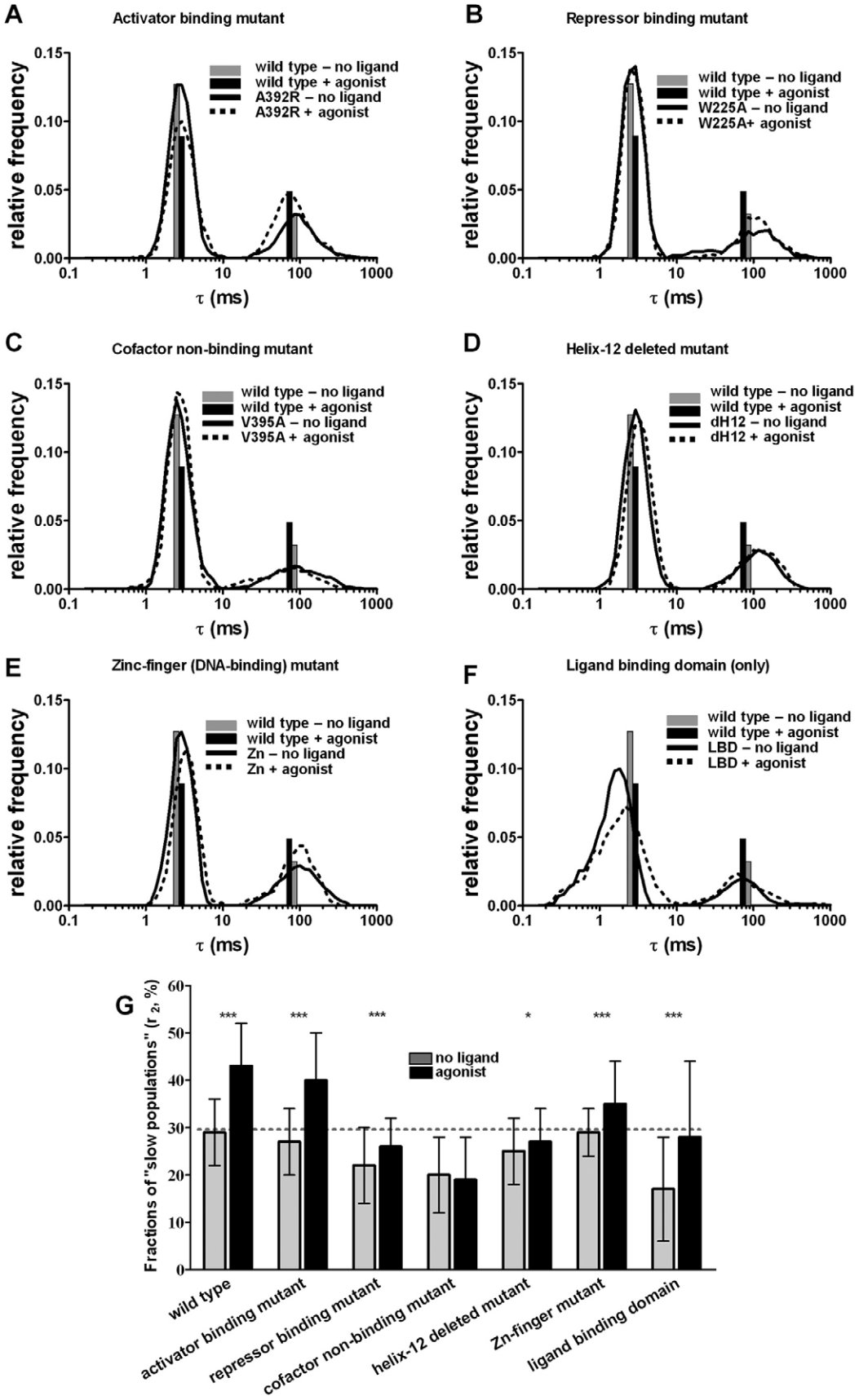

Fig. 6. See next page for legend.

similar to the wild type (data not shown). FCS measurements of nuclei transiently transfected with mutant forms of EGFP–RAR were carried out in the absence and presence of 100 nM AM580.

First we compared the diffusion properties of the untreated wild-type receptors and mutants with modified coregulator-binding. In the case of the 'activator-binding' mutant (A392R), the diffusion properties of the untreated receptor were similar to those of the wild type. On average, r_2=30% of the population showed slow diffusion before ligand treatment. Apparently, the loss of repressor binding did not have a dramatic effect on the dynamics of the receptor (Fig. 6A). By contrast, the increased SMRT-binding affinity of the 'repressor-binding' mutant (W225A) caused a slight increase in τ_2 and a slight decrease of r_2 (25%) for the untreated sample (Fig. 6B). The third, 'cofactor-non-binding' mutant (V395A) showed a further decreased level of r_2 (~20%) represented by a very low peak in the histogram (Fig. 6C).

The mutants showed a clearly disparate behavior after AM580-treatment. A clearly significant increase of r_2 (~12%) could only be detected in the case of the 'activator-binding' mutant, which behaved similarly to the wild type (Fig. 6G). The repressor-binding mutant had a smaller increase of r_2 (~4%), and no change was detected for the 'cofactor-non-binding' mutant. Based on these results we assumed that there is a strong connection between coactivator binding and the ligand-induced increase of the ratio of the slow population.

To further test this hypothesis, we studied the behavior of a mutant lacking the C-terminal helix 12 (H12) (Fig. 5B). H12 has a key role in the action of nuclear receptors as molecular switches. Upon ligand binding, it folds on the receptor similarly to the lever of a mouse-trap, forming a new interface for the coactivator to bind. Corepressor binding and active H12 conformation are mutually exclusive. Deletion of H12 results in a nonfunctional form of RAR that is unable to release the corepressor and bind coactivators. The diminished coactivator binding ability provided us with another aspect to investigate the connection between coactivator binding, activity and mobility of RAR. In the apo state, r_2 was slightly smaller for the ΔH12-mutant (26%) than for the wild type, and the increase of r_2 was nearly completely abolished (Fig. 6D,G). These features resemble the constitutive repressor-binding mutant, corroborating the connection between the ligand-induced redistribution of populations, coactivator binding capacity and activity (supplementary material Fig. S5). As seen from these results, mutations of the coregulator binding capacity changed the fraction of the slower, assumedly chromatin-bound component.

Fig. 6. Diffusion time distributions of the wild type and mutated forms of EGFP–RAR. (**A**) The activator-binding mutant (A392R, with elevated activator-binding affinity). (**B**) The repressor-binding mutant (W226A, with elevated repressor-binding affinity). (**C**) The cofactor non-binding mutant (V395A, with decreased coregulator-binding ability). (**D**) The helix-12 (AF2)-deleted mutant (with no ability for coregulator-exchange). (**E**) The Zn-finger mutant (with a reduced DNA-binding ability). (**F**) The ligand binding domain construct (LBD, with no direct DNA-binding capacity). Distributions of diffusion times of the mutant forms before (solid line) and 10 minutes after the addition (dotted line) of 100 nM AM580 are shown. Columns representing the wild type EGFP–RAR before (gray) and after (black) the addition of 100 nM AM580 are shown for comparison. The positions of the columns mark the average diffusion times (τ_1 and τ_2), and the heights of the columns are equal to the heights of the peaks shown in Fig. 3B of wild-type EGFP–RAR. (**G**) Summary of the changes in population ratios of wild-type and mutant forms of EGFP–RAR. See Table 1 for detailed results. (Data are means ± s.d., ***P<0.001; *P<0.1.)

Next, we tested mutants where the DNA-binding affinity of the receptor was directly altered.

Impaired DNA-binding gradually reduces the slow population, but does not abolish ligand-induced redistribution of populations

The DNA-binding domain of RAR has two zinc-finger motifs, each with four coordinating cysteine residues (Fig. 5). Mutation of all four cysteines to alanines in the first zinc finger led to a dramatic decrease in the activating capacity of the receptor, as demonstrated by the transient transfection analysis (supplementary material Fig. S5). The zinc-finger mutant showed nuclear localization when transfected into HeLa cells. According to the FCS measurements, this mutant behaved similarly to the wild type RAR: 29% of the unliganded receptors belonged to the slower population, but only a slight increase (6%) was measured after ligation. The change of distribution was smaller, but still statistically significant (Fig. 6E,G).

To completely abolish the direct DNA-binding capacity of the receptor, we examined the properties of the EGFP-tagged ligand-binding domain (LBD) of RAR (Fig. 5). Interestingly, this molecule still had residual activity (supplementary material Fig. S5) and showed a ligand-induced increase of r_2. As presented in the diffusion time distribution histogram, losing almost one half of the receptor and its direct DNA-binding capacity yielded a characteristic change. The ratio of the slower population in the untreated sample dropped to 17%. At the same time, an activation-dependent increase of r_2 could still be detected, but reached a significantly lower level (27%) than that of the full-length receptor (Fig. 6F). Because the LBD has no direct DNA-binding capacity, the ligand-induced redistribution to the slow state is probably due to dimer formation with RXR and binding to DNA through its dimerization partner. The fractions of the slow populations of the different mutant forms of EGFP–RAR with or without agonist treatment are summarized in Fig. 6G and Table 1. In summary, direct binding to chromatin is an important factor in determining the distribution of receptors among the fast and slow populations, but it is not the key determinant factor in the ligand-induced redistribution.

Full-length coactivator binding is indispensable for ligand-enhanced increase of the slow population

To gain more direct evidence for the role of cofactor binding in the distribution among the fast and slow states of RAR, we carried out competition experiments. We cotransfected mCherry-labeled, short coregulator peptides, the nuclear receptor binding interaction domains (IDs) of coregulators with an additional consensus nuclear localization signal: mCherry-NLS-ACTR-ID1+2 and mCherry-NLS-SMRT-ID1+2. These IDs bind to both members of the RAR–RXR dimer, but lack the domains responsible for docking further proteins of the transcription machinery. We monitored the expression level of the peptides through the fluorescence of mCherry. Labeled coregulator IDs showed nuclear localization (data not shown). The receptor-binding ability of the peptides was proven by the two-hybrid system competition assay (supplementary material Fig. S6).

Cotransfection of either coregulator-peptide (ACTR-ID coactivator and SMRT-ID corepressor) decreased r_2 by ~5% in the absence of ligand as compared with the wild type, and as the graph in Fig. 7A shows, it caused no major changes in the diffusion time distribution of unliganded receptors. It seems that

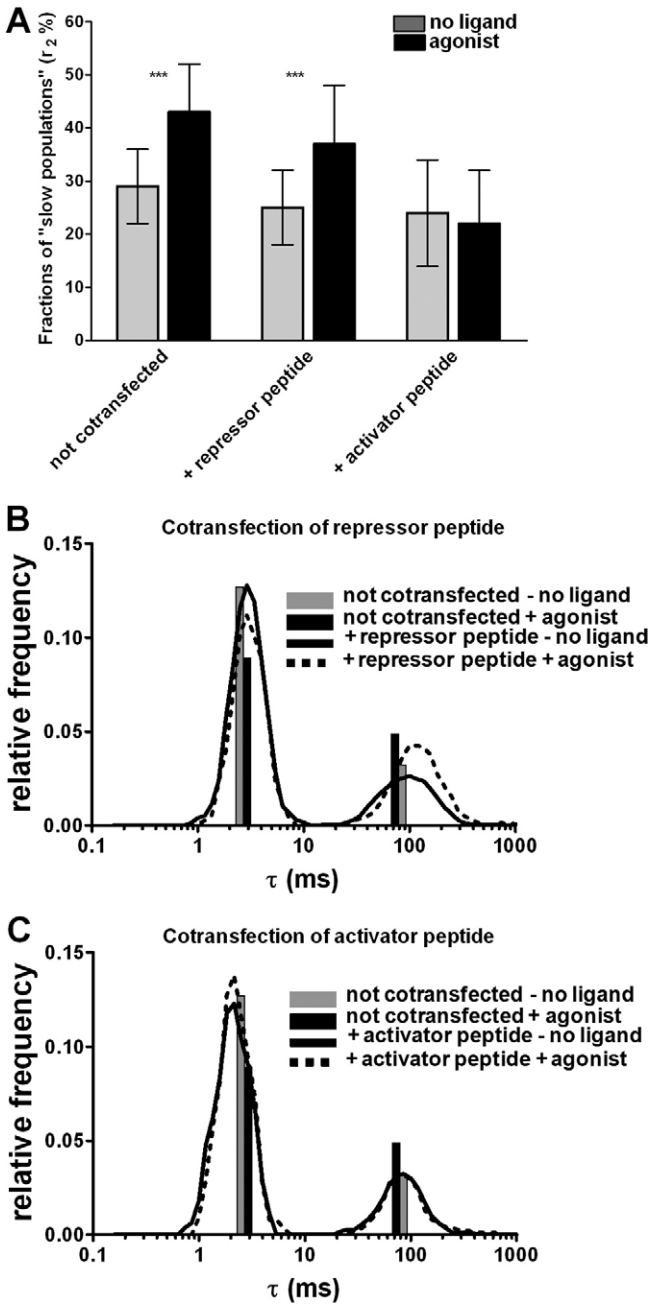

Fig. 7. The effect of cotransfected coregulator peptides on the ligand-induced r_2-increase of EGFP–RAR. (**A**) Ratios of the slow population (r_2) of EGFP–RAR alone or with the cotransfection of repressor peptide (mCherry-NLS-SMRT-ID1+2) or activator peptide (mCherry-NLS-ACTR-ID1+2) respectively, before (gray) and 10 minutes after (black) the addition of 100 nM AM580 (data are mean ± s.d.; ***$P<0.001$). (**B**) Distribution of diffusion times of EGFP–RAR with or without the cotransfection of repressor peptide (mCherry-NLS-SMRT-ID1+2). (**C**) Distribution of diffusion times of EGFP–RAR with or without the cotransfection of activator peptide (mCherry-NLS-ACTR-ID1+2). Columns representing the wild type EGFP–RAR before (gray) and after (black) the addition of 100 nM AM580 are shown for comparison. The positions of the columns mark the average diffusion times (τ_1 and τ_2), and the heights of the columns are equal to the heights of the peaks shown in Fig. 3B of wild-type EGFP–RAR.

receptors behave similarly in the presence of full-length corepressor or the short repressor ID in the absence of ligand. In the presence of ligand, the repressor peptide probably dissociates, giving way to agonist-induced binding of the coactivator, which is similar to the case when no repressor peptide was cotransfected (Fig. 7A,B). By contrast, when coactivator peptide is cotransfected, the agonist induced increase of r_2 is not observed (Fig. 7A,C). Binding of the short interaction domain of the activator is insufficient to the formation of the full activation complex. These results are consistent with our assumption that the ligand-induced redistribution between the fast and slow populations depends on binding full-length coactivator.

Discussion

The use of modern fluorescence microscopy techniques in transcription regulation research has allowed the mobility and interactions of molecules inside the cell to be assessed (Houtsmuller and Vermeulen, 2001; Lippincott-Schwartz et al., 2001; Schwille, 2001; van Roessel and Brand, 2002). A good example of the progress made is the case of the estrogen receptor (ERα). This receptor has been extensively studied and its nuclear localization and agonist-dependent speckle formation were described (Stenoien et al., 2000). Moreover, multiple diffusion components have been resolved using fluorescence microscopy techniques; primarily FRAP and FCS (Jankevics et al., 2005). Using FRAP measurements it was shown that unliganded ERα exhibited high mobility, and agonist treatment resulted in slower recovery of fluorophore-fused ERα after bleaching compared with the untreated state. It was also shown that the CFP–lacER chimera, which is immobilized at the *lac* promoter, can trigger agonist-dependent immobilization of SRC-1 activator by binding it to the nuclear receptor (Stenoien et al., 2001). The high intranuclear mobility of both nuclear receptors and coregulators was demonstrated for GR and GRIP-1 in another system (Becker et al., 2002). Biphasic models for the evaluation and fitting of FRAP curves were suggested, reflecting the scanning motion and transient engagement of proteins (Karpova et al., 2004). Based on these and other studies, as well as experiments with an MMTV-promoter array, the so called hit-and-run model was proposed (McNally et al., 2000). The FCS method allows the determination of local diffusion times of fluorescently labeled molecules. Diffusion time distribution analysis showed that co-existence of different states of the same nuclear receptor (ER) results in populations with distinct diffusion times (Jankevics et al., 2005). Three major states were described, namely small complexes and dimers; ligand-induced larger complexes; and the chromatin-bound population. Based on FRAP analysis of various chromatin proteins (structural, remodeling, coactivators, transcription factors) transient binding with characteristic short and long residence times was suggested (Phair et al., 2004). In this scenario, stably formed protein–protein or protein–DNA complexes are replaced by highly mobile, stochastically formed complexes. The dynamic concept of gene expression is largely influenced by the time resolution of available methods. The concept of transcription factors that cycle in a 30–60 minute period is mainly based on chromatin immunoprecipitation results. This is complemented by FRAP measurements, which add a new dimension of molecular dynamics. Although several studies have been carried out on nuclear receptors using the repertoire of fluorescence microscopy, the picture is not yet complete. FCS

can further increase the time resolution of these studies, yielding well-defined diffusion times in the millisecond range.

In this article we focused on RAR and described the characteristic features of RAR mobility. EGFP-fused RAR showed nuclear localization just like PPARs, RXR and TR (Akiyama et al., 2002; Maruvada et al., 2003). Speckle formation is a typical phenomenon that is not always interpreted the same way. In most cases, the flakes formed by nuclear receptors turned out to be pools of proteins caused by overexpression (Feige et al., 2005). We did not detect any speckle formation either in the absence or in the presence of agonist ligand, which shows that the expression level was low enough not to perturb the normal spatial distribution of the receptor in the nucleus. Transcriptional activities of the EGFP-tagged chimeras were virtually identical to the non-tagged forms when tested in transient transfection assays.

In FCS, finding the appropriate diffusion model is a critical issue. Several models have been applied in different studies, examining GR, PPAR and other transcription factors such as Jun and Fos (Baudendistel et al., 2005; Vamosi et al., 2008). These included free-diffusion models with one, two or three components and also anomalous diffusion models (Mikuni et al., 2007; Tudor et al., 2007). The latter is described by the anomaly coefficient (α), $\alpha=1$ representing free diffusion. The case $\alpha<1$ is called anomalous subdiffusion, which can be caused by molecular crowding or transient binding. Fitting our autocorrelation curves to the two-component free-diffusion model resulted in the least noisy residual curves with the best fit, as mentioned above. In good correlation with the earlier NR mobility studies discussed above, our FCS measurements described a two-component system with average diffusion times of 1.5–5 mseconds and 75–150 mseconds. These populations might represent the receptors in smaller diffusing complexes (monomers, dimers, small regulator complexes or a mixture of these) and ones that are bound to larger complexes and/or exhibit a stronger affinity towards the chromatin (and are likely to be transiently bound to it). It is important to point out that, from a biological perspective, the difference between a one-component anomalous and a two-component free diffusion model is minute. Assuming two distinct components (Jankevics et al., 2005) is justified if we consider that the receptor can be in (at least) two different states, e.g. as a monomer, dimer or small complex, or as part of a repressor–activator complex bound transiently or stably (on the time scale of FCS) to the chromatin. However, the one-component anomalous diffusion model (Gelman et al., 2006) also assumes stochastic transient binding, resulting in some molecules diffusing more slowly across the detection volume, whereas others that escape binding diffuse faster, broadening the decay of the autocorrelation curve. Thus, both models can describe the system appropriately.

In previous FRAP studies (Maruvada et al., 2003; Gelman et al., 2006), no increase in the average diffusion time of RAR was detected after agonist treatment, in contrast to ER, AR or GR (Dong et al., 2004). Here we reported a characteristic increase by 10%, resulting in a final value of 40% of the slow population of RAR. The described agonist-induced effect on RAR mobility can only be seen by FCS, and appears to be undetectable by FRAP. We suggest that this slow population includes the transcriptionally competent fraction of the receptors.

Besides characterization of the diffusion properties of the receptor, we also sought to find the main determinants that affect these properties. We created a set of point mutants to probe this. The mutations that resulted in a reduced activator binding ability (repressor-binding mutant and H12-deleted mutant) caused the loss of agonist-dependent increase in r_2, but also caused a slight increase in τ_2 and a slight decrease of r_2, in the unliganded state. A plausible explanation for this effect could be that, owing to its higher corepressor binding affinity (smaller k_{off}), these mutants might spend more time bound to the corepressor, thereby reducing the number of corepressors available at any given time point. Therefore, the r_2 fraction of receptors participating in corepressor complexes in the time window of FCS ($\sim$100 mseconds) decreases, and the apparent diffusion time τ_2 of the receptors within corepressor complexes increases. This latter phenomenon can also be an indication of the increased affinity of the receptor–corepressor complex to the chromatin compared with that of the receptor not binding corepressor. This notion is also supported by the reduced r_2 of the cofactor-non-binding mutant.

We showed that the loss of direct DNA-binding ability had a significant effect on the redistribution among fast and slow populations. The protein containing only the LBD of the receptor also showed an increase in r_2, but τ_2 became shorter, suggesting that the residence time on chromatin was reduced. Owing to the fact that the LBD has no direct DNA-binding capacity, DNA binding is probably facilitated by RXR, the heterodimerization partner of RAR. The DNA-binding affinity of RXR alone is apparently lower than that of the intact RAR–RXR dimer, resulting in a shorter residence time (shorter τ_2) on the chromatin. Interestingly, for LBD, τ_1 is also reduced compared with wild-type RAR, which cannot be explained by its smaller molecular mass alone; rather the LBD resides in the low-mobility complexes (bound to chromatin, or to coregulators) for shorter time spans. The shortening of τ_1 as a result of the loss of the DNA-binding domain might also indicate that the wild-type receptor is transiently bound to chromatin, not only in the slow state but, with a much reduced residence time, also in the fast state. This might explain why the fast component of the wild-type receptor is found to be slower than would be expected for a freely diffusing monomer.

The most likely and our favored scenario is that the ligand-induced increase of the slower population is very closely linked to coactivator binding (Fig. 8). By cotransfecting the interaction domains of the coactivator to RAR, we have managed to compete the endogenous coactivators from the receptors in the ligand-binding state, thus abolishing the redistribution of populations. In the presence of the endogenous full-length coactivators, the formation of the complete, functional coactivator complex is possible (by binding of further proteins); however, the coactivator-interaction domain lacks the binding surfaces for the additional components of the complex. Thus, the peptide-bound receptors cannot seed the full activator complex, and this is why the described redistribution of receptors cannot be detected. In this regard, it is important to note the unique nature of RAR among nuclear receptors: it is very potent in mediating both repression and activation of transcription. Therefore, the differences between the actions of nuclear receptors have to be taken into consideration when formulating a general concept of transcription dynamics.

Our conclusion is that the detected, agonist-dependent increase in the ratio of the slower population shows correlation with coactivator binding (and possibly dimerization). We would like to put forward the model that the key determinants of RAR

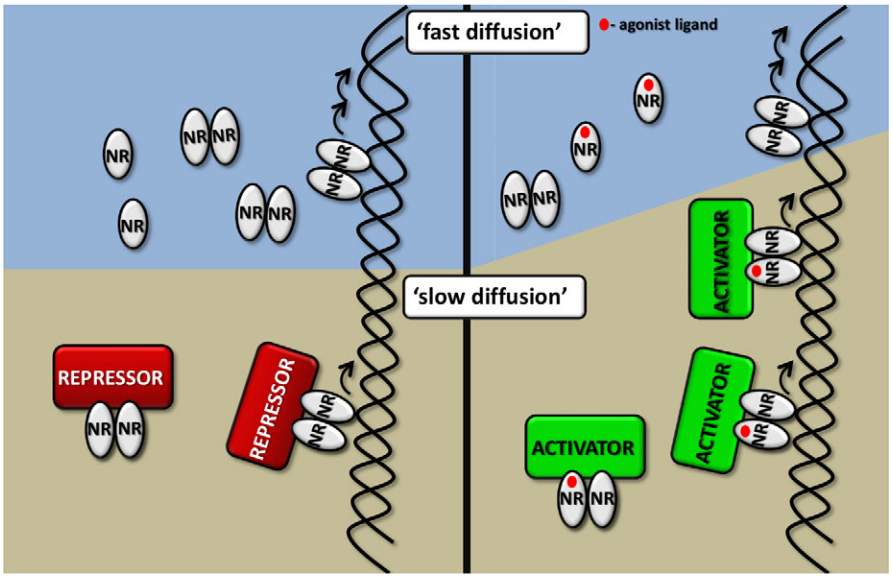

Fig. 8. Interpretations of the different states and populations of RAR as detected by FCS. The nucleus is depicted here in the absence (left side) or presence of a ligand for RAR. Left, the majority of the receptors (NR) in their unliganded state are present in a monomeric/dimeric form or as small complexes (the latter species is not shown in the figure). Freely diffusing receptors and maybe DNA-scanning receptors with short residence times on DNA represent the 'fast diffusing population' (upper, blue-shaded area). The 'slow population' (lower, brown-shaded area) probably corresponds to repressor-bound molecules, which can probably bind to chromatin with longer residence times than the ones in the 'fast population'. Right, the fraction of this slow population is increased when the receptor binds an agonist (red dot). In the activated state the size of the population that exhibits a longer residence time on chromatin and interacts with activator proteins increases (as indicated by the larger brown area).

mobility in the nucleus are chromatin-binding and receptor-coregulator interactions. Without the activating signal, the scanning activity dominates, which means that the equilibrium of populations of molecules with different diffusion times is mainly determined by weak, transient chromatin binding. However, coregulator binding is also present in this state, and becomes more pronounced when activation takes place. As the agonist ligand is bound to the ligand-binding pocket of the receptor, and it changes the conformation of the LBD, the coregulator-exchange can take place and coactivator is bound. This exchange affects the interaction of not only two proteins, but the entire complex of proteins. This change of the local nuclear environment results in a higher DNA-binding affinity of the receptor, replacing the scanning-like weak binding with a potentially stronger one that might consequently lead to the activation of the basic transcriptional machinery and the initiation of transcription. Obviously, this model needs refinement and further testing by FCS as well as FCCS or FRET techniques, in which co-mobility and colocalization of the receptors with cofactors as well as chromatin proteins and DNA should be determined.

Materials and Methods

Cell culture and transfection

RAR mobility was studied in live HeLa cells. Cells were maintained in Phenol-Red-free RPMI, supplemented with 10% fetal calf serum, 2 mM glutamine, penicillin and streptomycin. Cells were plated 48 hours before measurement into Nunc eight-well coverglass plates. 24 hours later, at 70% confluency, transfection was performed using 40 ng DNA mixed with 0.16 µl FuGene (Roche) per well.

A stable transfectant cell line of EGFP–RAR was created by G418 selection. HeLa cells were transfected with EGFP–hRARα plasmids using FuGene in T25 flasks. Two days later dead cells were removed and the original culture was diluted and moved to separate 25 cm^2 Petri dishes. After 2 days of culture neomycin selection was applied, and passaged cells were cultured with 800 µg/ml G418 (Sigma) from this point. Selective medium was refreshed every other day and cells were passaged every 4 days. This selection was continued for 3 weeks to remove most of the EGFP–RAR-negative cells. After the selection period, one week was allowed for colony formation. Each colony thus contained the descendants of one stably transfected cell. Colonies were picked from the Petri dishes using cloning rings, and were plated in 24-well plates. Several colonies were picked and cultured to reach at least 80% confluency inside the wells. The ratio of EGFP–RAR positive to negative populations and the distribution of intensity levels of the colonies were characterized by flow cytometry. A population with a narrow distribution of EGFP–RAR expression was sorted and propagated for subsequent experiments.

Plasmid constructs

cDNAs encoding human RARα, human RARα-LBD (containing only the ligand-binding domain), human RARα-ΔH12 (lacking helix-12 responsible for activator binding), cofactor interaction domains with nuclear localization signal NLS-hSMRT-ID and NLS-hACTR-ID (Benko et al., 2003) were subcloned after PCR amplification into pEGFP–C3 (Clontech) and pmCherry-C3 (created from pEGFP–C3 by replacing EGFP with mCherry) using *Bgl*II and *Hin*dIII for RAR constructs, *Xho*I and *Hin*dIII for SMRT, and *Nhe*I and *Sac*I for ACTR constructs. EGFP–RAR mutants were created using the QuikChange Site-Directed Mutagenesis Kit (Stratagene) according to the manufacturer's instructions. Integrity of all plasmids was confirmed by DNA sequencing. Expression vectors for transient transfection assays, Gal-SMRT-ID1+2, VP-hRARα-LBD, CMX-hRARα, pMH100-TK-luc, bRARE-luc, pCMX-β-galactosidase, Gal-ACTR-ID1+2, were described previously (Chen and Evans, 1995) and were kindly provided by Ronald M. Evans (Salk Institute for Biological Studies, La Jolla, CA, USA).

Transient transfection assay

Functional characterization of proteins was performed by cotransfecting 500 ng of the cDNA with 120 ng of reporter retinoic acid response element (RARE) and 90 ng of the β-galactosidase plasmid into COS-1 cells in 96-well plates. Luciferase activity was determined in the lysates using the Luciferase Assay Kit (Promega). Measurements were made with a Wallac Victor2 multilabel counter. The detected fluorescence is proportional to the transactivating ability of RARE-bound RAR. The signal of each sample was normalized to β-galactosidase activity to take the transfection efficiency and cell viability into account. Transient transfections were carried out in triplicate (Nagy et al., 1999).

Real-time RT-PCR

Total RNA was isolated with TRIzol reagent. Reverse transcription was performed at 42℃ for 1 hour and 72℃ for 5 minutes from 200 ng of total RNA using Superscript II reverse transcriptase. Quantitative PCR was performed, as reported previously (Szatmari et al., 2006).

Immunofluorescence detection of RAR in non-transfected and stably transfected (sGFP–RAR) cells

Cells were fixed with 3.7% formaldehyde (4℃, 10 minutes), permeabilized with 0.25% Triton and 0.1% TWEEN/TBS (room temperature, 30 minutes), blocked with 2% BSA with 0.1% TWEEN/TBS (room temperature, 30 minutes). Cells were then incubated with rabbit polyclonal anti-RARα antibody (C-20, Santa Cruz Biotechnologies, Santa Cruz, CA) at 1:200 dilution (room temperature, 1 hour), followed by incubation with ATTO633-conjugated anti-rabbit IgG for 1 hour at room temperature. Between consecutive steps cells were washed three times with PBS. Confocal images of labeled cells were taken with an Olympus FV1000 confocal microscope (EGFP fluorescence, Ex. 488 nm, Em. 500–530 nm; ATTO633, Ex. 633 nm, Em. 650–750 nm). Average pixel intensities in uniformly sized ROIs were determined with the ImageJ software and were corrected for background by subtracting the average intensity of cells incubated with the secondary antibody alone. Relative expression levels of the non-transfected and transfected cell lines were compared based on the corrected average intensities.

Pulsed ligand treatment

Transfected cells were incubated with 100 nM AM580 ligand in serum-free medium for 10 minutes before FCS measurements. FCS measurements (see next section) were carried out for 40 minutes afterwards. After washing out the ligand with pre-warmed (37℃) HBSS-buffer cells were kept in serum-free medium in a CO_2 incubator at 37℃ for 20 minutes. FCS measurements were then carried out in the absence of ligand for 40 minutes. Cells were treated again with ligand, and after incubation for 10 minutes they were measured with FCS.

Fluorescence correlation spectroscopy instrumentation and measurements

FCS measurements were performed on a modified Olympus FluoView 1000 confocal microscope based on an inverted IX-81 stand with an UPlanAPo 60× NA 1.2 water immersion objective. The two-channel FCS extension (prototype designed by Jörg Langowski, Steinbeis Transfer Center for Biophysical Analytics, Heidelberg, Germany) is attached to the fourth detection channel of the confocal scanning unit. FCS measurements on live HeLa cells were performed in eight-well chambered coverglass plates described above. Fluorescence of EGFP was excited by the 488 nm line of an Ar ion laser, and emission was detected through a 500–550 nm band-pass filter by a Perkin-Elmer avalanche photodiode (Perkin-Elmer, Wellesley, MA). Fluorescence autocorrelation curves were calculated online by an ALV-5000E correlator card (ALV-Laser Vertriebsgesellschaft, Langen, Germany). Measurements of 10×8 second runs were taken at three selected points in the nucleus of each selected cell.

Data analysis

'Good' autocorrelation curves from the 10×8 second runs were selected and averaged by the Correlation Run Select software (written by Károly Módos, Semmelweis University, Budapest, Hungary). Runs displaying large deviations from the average correlation curves because of rare events (large fluorescence fluctuations caused e.g. by aggregates) were excluded from the analysis. Nonlinear fitting of multiple runs at a selected point was carried out on the averaged autocorrelation curves using the QuickFit software (by Michael Tewes and Malte Wachsmuth, DKFZ, Heidelberg, Germany). For fitting the autocorrelation curves of EGFP-labeled RAR molecules a model with two diffusion components, triplet correction and a term taking account of EGFP blinking was used:

$$G(\tau)=\frac{1-T-\Theta_c+Te^{-\tau/\tau_{tr}}+\Theta_c e^{-\tau/\tau_c}}{1-T-\Theta_c}G_{diff} \quad (1)$$

where

$$G_{diff}^{free}(\tau)=\frac{1}{N}\left[r_1\left(1+\frac{\tau}{\tau_1}\right)^{-1}\left(1+\frac{\tau}{S^2\tau_1}\right)^{-1/2}+r_2\left(1+\frac{\tau}{\tau_2}\right)^{-1}\left(1+\frac{\tau}{S^2\tau_2}\right)^{-1/2}\right] \quad (2)$$

$$G_{diff}^{anomal}(\tau)=\frac{1}{N}\left[r_1\left(1+\left(\frac{\tau}{\tau_1}\right)^{\alpha_1}\right)^{-1}\left(1+\frac{1}{S^2}\left(\frac{\tau}{\tau_1}\right)^{\alpha_1}\right)^{-1/2}+r_2\left(1+\left(\frac{\tau}{\tau_2}\right)^{\alpha_2}\right)^{-1}\left(1+\frac{1}{S^2}\left(\frac{\tau}{\tau_2}\right)^{\alpha_2}\right)^{-1/2}\right] \quad (3)$$

The autocorrelation function can be broken down to a term accounting for triplet state formation and dark state formation due to protonation (or light-induced transition to a non-emitting state) also called blinking, and a term accounting for diffusion (G_{diff}). N is the average number of dye molecules in the detection volume, τ is the lag time. In the triplet term T denotes the equilibrium molar fraction of fluorophores in the triplet state and τ_{tr} is the triplet lifetime (Widengren and Rigler, 1998). Two independent protonation mechanisms: an intramolecular proton transfer and a pH-dependent external protonation process have been described (Haupts et al., 1998). Because the characteristic time constants of the two protonation processes are separated by less than an order of magnitude at pH 7.4, a single term, characterized by the molecular fraction $\boldsymbol{\Theta}_c$ and the correlation time τ_c was considered.

In the diffusion terms G_{diff}^{free} and G_{diff}^{anomal} the diffusion of two species has been assumed: a fast one with a mole fraction r_1 and diffusion time τ_1, and a slow one with a mole fraction $r_2=1-r_1$, and diffusion time τ_2. Including a third diffusion component did not improve the fit significantly and yielded very low amplitudes for the third component, rendering the fit unreliable. S denotes the ratio of the longitudinal vs. radial diameters of the ellipsoid-shaped detection volume (defined by the surface of e^{-2} detection efficiency relative to the center of the illuminated spot). The exponent α accounts for the mechanism of diffusion; $\alpha=1$ for free (Brownian) diffusion, $\alpha<1$ for obstructed diffusion (Wachsmuth et al., 2000). For free diffusion, the mean-squared displacement is a linear function of the time, i.e. the diffusion coefficient is independent of the traveled distance. Anomaly means that the diffusion coefficient becomes exceedingly smaller for diffusion over longer distances. Anomalous diffusion can result from transient binding or molecular crowding.

The diffusion of EGFP in the nucleus was fitted to a single-diffusion component model with triplet and blinking correction. Histograms of diffusion time distributions were created as follows. Each decade was divided to five bins having equal width on a logarithmic scale. τ_1 and τ_2 values derived from the nonlinear fits contributed to the appropriate bins (containing τ_1 or τ_2) by the weights of the components, r_1 and r_2, respectively. To make histograms smoother, the bins were shifted in five equal steps on a log scale, and in each step the actual height was assigned to the centre of the bin. Finally, the sum of the frequencies of all bins was normalized to unity. Thus, the relative frequencies belonging to the peak of the fast or slow diffusion time add up to r_1 and r_2, respectively. This procedure resulted in an optimal nonparametric estimator of the probability density function of our data (Venables and Ripley, 1997). The average weights of the slow fraction, r_2, were also presented as bar graphs.

The diffusion coefficient D_i (i=1,2) of a fluorescent species can then be assessed as:

$$D_i=\omega_{xy}^2/(4\tau_i) \quad (4)$$

where ω_{xy} is the lateral radius of the detection volume. ω_{xy} at 488 nm excitation was estimated from the diffusion of Alexa Fluor 488 (50 nM solution dissolved in 10 mM Tris-EDTA buffer, pH 7.4), and calculating $\omega_{xy}=\sqrt{4D\tau_D}=\sqrt{4\times 414\mu m^2/s\times 22\mu s}\sim 191$ nm, where D was taken from the literature (D=414 μm^2/second at 25℃) (Petrov, 2008).

The apparent molecular mass of the receptor or receptor complex, assuming a spherical shape for the diffusing species was assessed from the diffusion times by using the following relation based on the Stokes–Einstein equation:

$$M_{EGFP-RAR}^{apparent}/M_{EGFP}=(D_{EGFP}/D_{EGFP-RAR})^3=(\tau_{EGFP-RAR}/\tau_{EGFP})^3 \quad (5)$$

where M_{EGFP}=27 kDa is the molecular mass of EGFP, and $\tau_{EGFP\text{-}RAR}$ and τ_{EGFP} are their respective diffusion autocorrelation times determined from the nonlinear fits.

Statistical analysis to compare the averages of best fit parameters was carried out with unpaired t-tests using the Graphpad Prism software. Comparison of different diffusion models was carried out with an F-test (one-component free diffusion vs two-component free diffusion, one-component free diffusion vs one-component anomalous diffusion) or with corrected Aikaike's information criteria (two-component free vs one-component anomalous diffusion) using an online calculator (Graphpad Software, http://www.graphpad.com/quickcalcs/AIC2.cfm).

Acknowledgements

We are grateful to Louise Fariall and John Schwabe (University of Leicester, UK) for help with structure interpretation and discussions and members of the Nagy laboratory for comments on the manuscript. We thank Márta Béládi and Ibolya Fürtös for technical assistance, Attila Horváth and Tamás Domoszlai for participation in FCS and transient transfection experiments and Gábor Mocsár for helpful discussions.

Funding

L.N. is an International Scholar of HHMI and holds a Wellcome Trust Senior Research Fellowship in Biomedical Sciences. This work was supported by grants from the Hungarian Scientific Research Fund OTKA [grant numbers NK72730 to L.N., K77600 to G.V.]; MOLMEDREX (FP7-REGPOT-2008-1) [grant number 229920 to L.N. and G.V.]; the German-Hungarian program for the exchange of researchers by the German Academic Exchange Service and the Hungarian Scholarship Board [grant numbers MÖB-47-1/2010 to G.V. and K.T., TÁMOP-4.2.2/08/1 to L.N., TÁMOP-4.2.1/B-09/1/KONV-2010-0007 to L.N. and G.V., TÁMOP 4.2.2.-08/1-2008-0019 to G.V.] implemented through the New Hungary Development Plan co-financed by the European Social Fund and the European Regional Development Fund. Deposited in PMC for release after 6 months.

Supplementary material available online at
http://jcs.biologists.org/lookup/suppl/doi:10.1242/jcs.086082/-/DC1

References

Akiyama, T. E., Baumann, C. T., Sakai, S., Hager, G. L. and Gonzalez, F. J. (2002). Selective intranuclear redistribution of PPAR isoforms by RXR alpha. *Mol. Endocrinol.* **16**, 707-721.

Axelrod, D., Koppel, D. E., Schlessinger, J., Elson, E. and Webb, W. W. (1976). Mobility measurement by analysis of fluorescence photobleaching recovery kinetics. *Biophys J.* **16**, 1055-1069.

Bacia, K. and Schwille, P. (2003). A dynamic view of cellular processes by in vivo fluorescence auto- and cross-correlation spectroscopy. *Methods* **29**, 74-85.

Baudendistel, N., Muller, G., Waldeck, W., Angel, P. and Langowski, J. (2005). Two-hybrid fluorescence cross-correlation spectroscopy detects protein-protein interactions in vivo. *Chemphyschem* **6**, 984-990.

Becker, M., Baumann, C., John, S., Walker, D. A., Vigneron, M., McNally, J. G. and Hager, G. L. (2002). Dynamic behavior of transcription factors on a natural promoter in living cells. *EMBO Rep.* **3**, 1188-1194.

Benko, S., Love, J. D., Beladi, M., Schwabe, J. W. and Nagy, L. (2003). Molecular determinants of the balance between co-repressor and co-activator recruitment to the retinoic acid receptor. *J. Biol. Chem.* **278**, 43797-43806.

Berland, K. M. (2004). Fluorescence correlation spectroscopy: a new tool for quantification of molecular interactions. *Methods Mol. Biol.* **261**, 383-398.

Brock, R., Vamosi, G., Vereb, G. and Jovin, T. M. (1999). Rapid characterization of green fluorescent protein fusion proteins on the molecular and cellular level by fluorescence correlation microscopy. *Proc. Natl. Acad. Sci. USA* **96**, 10123-10128.

Chen, J. D. and Evans, R. M. (1995). A transcriptional co-repressor that interacts with nuclear hormone receptors. *Nature* **377**, 454-457.

Darimont, B. D., Wagner, R. L., Apriletti, J. W., Stallcup, M. R., Kushner, P. J., Baxter, J. D., Fletterick, R. J. and Yamamoto, K. R. (1998). Structure and specificity of nuclear receptor-coactivator interactions. *Genes Dev.* **12**, 3343-3356.

Dong, S., Stenoien, D. L., Qiu, J., Mancini, M. A. and Tweardy, D. J. (2004). Reduced intranuclear mobility of APL fusion proteins accompanies their mislocalization and results in sequestration and decreased mobility of retinoid X receptor alpha. *Mol. Cell. Biol.* **24**, 4465-4475.

Feige, J. N., Gelman, L., Tudor, C., Engelborghs, Y., Wahli, W. and Desvergne, B. (2005). Fluorescence imaging reveals the nuclear behavior of peroxisome proliferator-activated receptor/retinoid X receptor heterodimers in the absence and presence of ligand. *J. Biol. Chem.* **280**, 17880-17890.

Gelman, L., Feige, J. N., Tudor, C., Engelborghs, Y., Wahli, W. and Desvergne, B. (2006). Integrating nuclear receptor mobility in models of gene regulation. *Nucl. Recept. Signal* **4**, e010.

Gottlicher, M., Heck, S. and Herrlich, P. (1998). Transcriptional cross-talk, the second mode of steroid hormone receptor action. *J. Mol. Med.* **76**, 480-489.

Haupts, U., Maiti, S., Schwille, P. and Webb, W. W. (1998). Dynamics of fluorescence fluctuations in green fluorescent protein observed by fluorescence correlation spectroscopy. *Proc. Natl. Acad. Sci. USA* **95**, 13573-13578.

Heery, D. M., Kalkhoven, E., Hoare, S. and Parker, M. G. (1997). A signature motif in transcriptional co-activators mediates binding to nuclear receptors. *Nature* **387**, 733-736.

Hermanson, O., Glass, C. K. and Rosenfeld, M. G. (2002). Nuclear receptor coregulators: multiple modes of modification. *Trends Endocrinol. Metab.* **13**, 55-60.

Hess, S. T. and Webb, W. W. (2002). Focal volume optics and experimental artifacts in confocal fluorescence correlation spectroscopy. *Biophys. J.* **83**, 2300-2317.

Hinojos, C. A., Sharp, Z. D. and Mancini, M. A. (2005). Molecular dynamics and nuclear receptor function. *Trends Endocrinol Metab* **16**, 12-18.

Houtsmuller, A. B. and Vermeulen, W. (2001). Macromolecular dynamics in living cell nuclei revealed by fluorescence redistribution after photobleaching. *Histochem. Cell Biol.* **115**, 13-21.

Jankevics, H., Prummer, M., Izewska, P., Pick, H., Leufgen, K. and Vogel, H. (2005). Diffusion-time distribution analysis reveals characteristic ligand-dependent interaction patterns of nuclear receptors in living cells. *Biochemistry* **44**, 11676-11683.

Karpova, T. S., Chen, T. Y., Sprague, B. L. and McNally, J. G. (2004). Dynamic interactions of a transcription factor with DNA are accelerated by a chromatin remodeller. *EMBO Rep.* **5**, 1064-1070.

Lippincott-Schwartz, J., Snapp, E. and Kenworthy, A. (2001). Studying protein dynamics in living cells. *Nat. Rev. Mol. Cell Biol.* **2**, 444-456.

Lippincott-Schwartz, J., Altan-Bonnet, N. and Patterson, G. H. (2003). Photobleaching and photoactivation: following protein dynamics in living cells. *Nat. Cell Biol*. **Suppl**, S7-S14.

Love, J. D., Gooch, J. T., Benko, S., Li, C., Nagy, L., Chatterjee, V. K., Evans, R. M. and Schwabe, J. W. (2002). The structural basis for the specificity of retinoid-X receptor-selective agonists: new insights into the role of helix H12. *J. Biol. Chem.* **277**, 11385-11391.

Mangelsdorf, D. J., Thummel, C., Beato, M., Herrlich, P., Schutz, G., Umesono, K., Blumberg, B., Kastner, P., Mark, M., Chambon, P. et al. (1995). The nuclear receptor superfamily: the second decade. *Cell* **83**, 835-839.

Maruvada, P., Baumann, C. T., Hager, G. L. and Yen, P. M. (2003). Dynamic shuttling and intranuclear mobility of nuclear hormone receptors. *J. Biol. Chem.* **278**, 12425-12432.

McNally, J. G., Muller, W. G., Walker, D., Wolford, R. and Hager, G. L. (2000). The glucocorticoid receptor: rapid exchange with regulatory sites in living cells. *Science* **287**, 1262-1265.

Metivier, R., Reid, G. and Gannon, F. (2006). Transcription in four dimensions: nuclear receptor-directed initiation of gene expression. *EMBO Rep.* **7**, 161-167.

Mikuni, S., Tamura, M. and Kinjo, M. (2007). Analysis of intranuclear binding process of glucocorticoid receptor using fluorescence correlation spectroscopy. *FEBS Lett.* **581**, 389-393.

Nagy, L., Kao, H. Y., Love, J. D., Li, C., Banayo, E., Gooch, J. T., Krishna, V., Chatterjee, K., Evans, R. M. and Schwabe, J. W. (1999). Mechanism of corepressor binding and release from nuclear hormone receptors. *Genes Dev.* **13**, 3209-3216.

Onate, S. A., Tsai, S. Y., Tsai, M. J. and O'Malley, B. W. (1995). Sequence and characterization of a coactivator for the steroid hormone receptor superfamily. *Science* **270**, 1354-1357.

Petrov, E. P., Schwille, P. (2008). State of the art and novel trends in fluorescence correlation spectroscopy. In *Standardization and Quality Assurance in Fluorescence Measurements: State of the Art and Future Challenges*.Berlin, Heidelberg, New York: Springer.

Phair, R. D., Scaffidi, P., Elbi, C., Vecerova, J., Dey, A., Ozato, K., Brown, D. T., Hager, G., Bustin, M. and Misteli, T. (2004). Global nature of dynamic protein-chromatin interactions in vivo: three-dimensional genome scanning and dynamic interaction networks of chromatin proteins. *Mol. Cell. Biol.* **24**, 6393-6402.

Rachez, C., Suldan, Z., Ward, J., Chang, C. P., Burakov, D., Erdjument-Bromage, H., Tempst, P. and Freedman, L. P. (1998). A novel protein complex that interacts with the vitamin D3 receptor in a ligand-dependent manner and enhances VDR transactivation in a cell-free system. *Genes Dev.* **12**, 1787-1800.

Schwille, P. (2001). Fluorescence correlation spectroscopy and its potential for intracellular applications. *Cell Biochem. Biophys* **34**, 383-408.

Sprague, B. L., Pego, R. L., Stavreva, D. A. and McNally, J. G. (2004). Analysis of binding reactions by fluorescence recovery after photobleaching. *Biophys. J.* **86**, 3473-3495.

Stenoien, D. L., Mancini, M. G., Patel, K., Allegretto, E. A., Smith, C. L. and Mancini, M. A. (2000). Subnuclear trafficking of estrogen receptor-alpha and steroid receptor coactivator-1. *Mol. Endocrinol.* **14**, 518-534.

Stenoien, D. L., Nye, A. C., Mancini, M. G., Patel, K., Dutertre, M., O'Malley, B. W., Smith, C. L., Belmont, A. S. and Mancini, M. A. (2001). Ligand-mediated assembly and real-time cellular dynamics of estrogen receptor alpha-coactivator complexes in living cells. *Mol. Cell. Biol.* **21**, 4404-4412.

Szatmari, I., Vamosi, G., Brazda, P., Balint, B. L., Benko, S., Szeles, L., Jeney, V., Ozvegy-Laczka, C., Szanto, A., Barta, E. et al. (2006). Peroxisome proliferator-activated receptor gamma-regulated ABCG2 expression confers cytoprotection to human dendritic cells. *J. Biol. Chem.* **281**, 23812-23823.

Tudor, C., Feige, J. N., Pingali, H., Lohray, V. B., Wahli, W., Desvergne, B., Engelborghs, Y. and Gelman, L. (2007). Association with coregulators is the major determinant governing peroxisome proliferator-activated receptor mobility in living cells. *J. Biol. Chem.* **282**, 4417-4426.

Vamosi, G., Damjanovich, S., Szollosi, J. and Vereb, G. (2009). Measurement of molecular mobility with fluorescence correlation spectroscopy. *Curr. Protoc. Cytom.* **Chapter 2**, Unit 2. 15.

Vamosi, G., Baudendistel, N., von der Lieth, C. W., Szaloki, N., Mocsar, G., Muller, G., Brazda, P., Waldeck, W., Damjanovich, S., Langowski, J. et al. (2008). Conformation of the c-Fos/c-Jun complex in vivo: a combined FRET, FCCS, and MD-modeling study. *Biophys. J.* **94**, 2859-2868.

van Roessel, P. and Brand, A. H. (2002). Imaging into the future: visualizing gene expression and protein interactions with fluorescent proteins. *Nat. Cell Biol.* **4**, E15-E20.

Venables, W. N. and Ripley, B. D. (1997). Modern Applied Statistics with S-PLUS: Springer.

Wachsmuth, M., Waldeck, W. and Langowski, J. (2000). Anomalous diffusion of fluorescent probes inside living cell nuclei investigated by spatially-resolved fluorescence correlation spectroscopy. *J. Mol. Biol.* **298**, 677-689.

Widengren, J. and Rigler, R. (1998). Fluorescence correlation spectroscopy as a tool to investigate chemical reactions in solutions and on cell surfaces. *Cell. Mol. Biol. (Noisy-le-grand)* **44**, 857-879.

Table S1. Chi-squared values of the fits of wild type and mutated EGFP-RAR autocorrelation curves with different diffusion models

	AM580	one-component free	anomalous	two-component free
EGFP	-	41.9	37.2	21.3
EGFP-RAR	-	103.1	33.3	25.9
	+	80.2	35.4	25.7
EGFP-RAR-AR	-	91.3	33.7	24.2
	+	87.9	32.7	23.5
EGFP-RAR-VA	-	79.5	33.7	26.6
	+	76.7	30.6	26.1
EGFP-RAR-WA	-	89.0	59.0	21.4
	+	92.9	65.0	20.7
EGFP-RAR-dH12	-	77.4	26.1	20.4
	+	78.3	27.0	23.0
EGFP-RAR-LBD	-	65.5	35.9	21.8
	+	70.9	33.0	23.7
EGFP-RAR-mZN	-	68.0	28.9	24.9
	+	69.9	30.4	25.1

Table S2. Mobility parameters of wild-type and mutated EGFP-RAR with different diffusion models. Data represent the best-fit parameters to the one-component anomalous

	100 nM AM580	2-component free diffusion		
		_1 (ms)	_2 (ms)	r2
EGFP-RAR	-	2.64 ± 0.65	97 ± 57	29% ± 7%
EGFP-RAR	+	2.87 ± 0.99	89 ± 45	43% ± 9%
EGFP-RAR-A392R (activator binding mutant)	-	2.69 ± 0.73	108 ± 81	27% ± 8%
	+	2.83 ± 0.92	92 ± 56	39% ± 11%
EGFP-RAR-W225A (repressor binding mutant)	-	2.64 ± 1.07	119 ± 81	22% ± 8%
	+	2.54 ± 0.5	127 ± 80	26% ± 7%
EGFP-RAR-V395A (cofactor non-binding mutant)	-	2.66 ± 1.29	120 ± 112	20% ± 8%
	+	2.65 ± 0.84	116 ± 121	19% ± 9%
EGFP-RAR-dH12 (Helix-12 deleted mutant)	-	2.83 ± 0.81	120 ± 62	26% ± 7%
	+	3.17 ± 0.84	124 ± 58	27% ± 7%
EGFP-RAR-mZn (Zinc-finger mutant)	-	2.89 ± 0.7	105 ± 61	29% ± 6%
	+	3.40 ± 0.99	111 ± 61	35% ± 9%
EGFP-RAR-LBD (ligand binding domain only)	-	1.62 ± 0.62	99 ± 101	17% ± 11%
	+	2.05 ± 1.20	114 ± 138	27% ± 15%

Table S3. Comparison of RAR-expression in non-trasfected (HeLa) and stable transfectant (sGFP-RAR HeLa) cell lines based on confocal microscopic evaluation of fluorescence intensities from immunolabeled RAR

	Intensity	
	Mean	s.d.
Control	60	6
HeLa	225	19
sEGFP-RAR HeLa	380	38
Corrected		
HeLa	165	
sEGFP-RAR HeLa	320	
Ratio of expression *(sEGFP-RAR-HeLa/HeLa)*	2	